RSC Advances

PAPER

View Article Online
View Journal | View Issue

Cite this: *RSC Adv.*, 2025, **15**, 29978

Resistance mechanism of soluble microbial products to silver nanoparticles in activated sludge: adsorption, bonding and influencing factors

Jia Kang, *[a] Ao-di Wang,[a] Yao-wen Zhang,[b] Fei Dai,[a] Jing-jing Zhu,[a] Chu-qiong Song[c] and Gang-fu Song[a]

The extensive application of silver nanoparticles (AgNPs) has resulted in them ending up in wastewater treatment plant (WWTP) facilities at concentrations varying between 0.13 and 20.02 mg L^{-1}. Soluble microbial products (SMPs) in activated sludge systems can form the first barrier against AgNPs before attached metabolites and microorganisms react with these biotoxicants. Based on this, the present study investigated the adsorption and bonding resistance mechanisms of AgNPs on SMPs in activated sludge systems and analysed the typical influencing factors. Analysis using quasi-second-order kinetics and the Freundlich isotherm model revealed that the adsorption of AgNPs onto SMP is chemisorption-controlled, with multi-layer adsorption being the main mechanism, and the adsorption capacity reached 263.9 mg g^{-1} at 35 °C. Fourier-transform infrared spectroscopy and X-ray photoelectron spectroscopy analyses indicated that aldehydes, carbonyl groups, and amide groups in SMPs were able to interact with AgNPs through electrostatic forces, hydrogen bonding and chelate-forming, metal-bound organometallic complexes (M–C=NOHC=NOH–M), resulting in conformational changes in SMP proteins. An increase in pH and ionic strength favoured the resistance of SMPs to AgNPs, and as the valence of the metal cation increased, the enhancement of this resistance became more significant. This study confirmed that SMP functions as an effective natural adsorbent for immobilizing AgNPs in activated sludge systems and provides a mechanistic foundation for developing targeted *in situ* bioremediation strategies.

Received 12th May 2025
Accepted 7th August 2025

DOI: 10.1039/d5ra03336e

rsc.li/rsc-advances

1. Introduction

AgNPs are widely applied across diverse areas such as medical equipment, solar energy applications, household appliances, textiles, and cosmetics owing to their effective antibacterial properties and photoelectric characteristics.[1,2] After use, the nanoparticle products are discharged into WWTPs as part of the urban water cycle.[3,4] Investigative studies demonstrated that the concentration of AgNPs in WWTPs ranged from 0.13 mg L^{-1} to 20.02 mg L^{-1}, where WWTPs form a sink for AgNPs.[5] Through aggregation, precipitation and biosorption, activated sludge in WWTPs could effectively absorb and capture around 90% of AgNPs.[6] The ecotoxic substances captured in WWTPs, such as AgNPs, significantly impact the metabolic activity of activated sludge, thereby reducing the treatment efficiency of WWTPs.[7]

Biotoxicants such as AgNPs stimulate the oxidative-stress response mechanism of activated sludge.[8] The resistance of activated sludge to AgNPs and other cytotoxic substances is divided into three processes: extracellular adsorption, transmembrane transport, and intracellular interaction.[9] During extracellular adsorption, the primary components of microbial metabolites, such as proteins, polysaccharides, and humic acids, could present various functional groups, including methyl, amino, phosphoric acid, and sulfhydryl groups.[10] These groups are potential binding sites for the attachment of heavy metals. These functional groups (as potential binding sites) could decrease the concentrations of heavy metals from ppm to ppb levels within a few hours,[11,12] thus forming a first-response barrier against cytotoxic substances, which prevents toxic substances from infiltrating the cell interior. Consequently, extracellular adsorption safeguards the structure of microbial cells and maintains the stability of the biological treatment system.[13] In particular, microbial metabolites play a crucial role in assisting anaerobic bacteria to resist toxicity, with Cu^{2+} removal exceeding 80% at low Cu^{2+} and Zn^{2+} doses of less than 5 mg L^{-1}.[14] Transmembrane transport and intracellular interactions disrupt the cellular structure. Thus, the extracellular adsorption of microbial metabolites serves as a barrier against AgNPs within activated sludge.[15]

During microbial defence against AgNPs, SMP in activated sludge systems first reacts with biotoxicants, then binds to

[a]School of Environmental and Municipal Engineering, North China University of Water Resources and Electric Power, Zhengzhou 450046, China. E-mail: kangjia@ncwu.edu.cn
[b]Hubei Institute of Water Resources Survey and Design Co., Ltd, Wuhan 430070, China
[c]Henan Urban Planning and Design Institute Co., Ltd, Zhengzhou 450044, China

microorganisms to form the first resistance barrier.[16] Lu *et al.*[17] demonstrated the adsorption capabilities of SMP, tightly bound extracellular polymeric substances (TB-EPS), and bacterial cells on Pb^{2+}, Cu^{2+}, and Zn^{2+} in the *Desulfovibrio vulnificus* systems, where the adsorption capacity followed the order: SMP > TB-EPS > bacterial cells. In subsequent experiments, Sun *et al.*[18] investigated the binding affinity of Zn^{2+} and Co^{2+} with EPS in an aerobic sludge system, where the results revealed that SMP exhibited stronger binding properties compared to TB-EPS.

SMP exerts resistance mainly by interacting with cationic, cytotoxic substances such as AgNPs through major components, such as proteins, lipids, polysaccharides, and nucleic acids.[19] As demonstrated in relevant studies, SMP was confirmed as a moderate ligand for Cu^{2+} with chelation stability constants $\mathrm{Log}^{c}K$ of 7.6–8.8.[20] In contrast, proteins and humic acid-like components are strong ligands for Cu^{2+}, Fe^{3+}, and Al^{3+}.[21] SMP and cytotoxic substances bind to metal ions *via* hydrogen bonding or chelation to form organometallic compounds.[22] Humic-like substances in SMP combine with Ni^{2+} to create stable complexes in solution,[23] where SMP was able to precipitate up to 99% of the metal under short-term Ni^{2+}- and Co^{2+}-stress conditions.[24]

The presence of AgNPs in activated sludge systems compromises the operational stability,[25] primarily by inducing structural damage to microbial cells during biological treatment,[26,27] thereby impairing the system performance and pollutant removal efficiency. Consequently, elucidating the mechanisms of SMP resistance against cytotoxic AgNPs is critical. Currently, the adsorption and bonding mechanisms governing SMP resistance to AgNPs in activated sludge systems are still unclear. In this study, SMP was initially extracted from an activated sludge system and the kinetics and thermodynamics of adsorption of AgNPs on SMP were systematically investigated. Furthermore, multivariate analyses were employed to characterize the changes in the chemical structure of SMP during its interaction with AgNPs. Based on this, the effective mechanisms by which SMP resists AgNPs under different pH conditions and Na^{+}, Ca^{2+} ionic strengths were investigated. This study aims to provide theoretical and strategic support for the *in situ* management and control of SMP in relation to AgNPs in activated sludge systems.

2. Materials and methods

2.1. Extraction of SMP

The aerobic activated sludge used in the experiments was obtained from the aeration tank of the Wangxinzhuang Wastewater Treatment Plant in Zhengzhou, Henan Province. A 50 mL sample of aerobic activated sludge mixture was collected and centrifuged at 4000 rpm and 4 °C for 10 min. Subsequently, the supernatant obtained was filtered using 0.45 μm organic filter membranes to obtain the SMP solution.

2.2. Preparation of AgNPs

Citric-acid-coated AgNPs were synthesized *via* a chemical reduction technique. Briefly 0.5 mL of a 50 mM $AgNO_3$ solution and 0.75 mL of a 50 mM $C_6H_5Na_3O_7$ solution were introduced into 100 mL of distilled water (maintained at 45 °C). After sufficient stirring, 10 mL of a 5 mM $NaBH_4$ solution was added drop-by-drop to the mixture with high-speed stirring for 30 min, yielding a yellow-brown sol containing AgNPs.

The prepared AgNPs sol was removed from the water-bath, then sonicated for 20 min to disperse the nanoparticles and prevent oxidative aggregation. After cooling, the solution was stored at 4 °C and kept away from light.

2.3. Analysis of adsorption of AgNPs on SMP

2.3.1. Adsorption kinetics. In the adsorption kinetics experiments, the initial concentration of the adsorbent SMP was 8.4 mg L^{-1} (total organic carbon, TOC). The initial concentrations of the AgNPs were 3.774, 6.290, and 9.435 mg L^{-1}, respectively. In addition, the initial pH of the solutions was precisely controlled to 8.0. The experiments were conducted in a thermostatic shaking chamber (SHA-C, Changzhou Zhiborui Instrument Manufacturing Co., Ltd), with the temperature maintained at 25 °C and the rotational speed set at 120 rpm. Samples were collected at predetermined intervals (5, 10, 15, 20, 30, 60, 90, 120, 180, 240, 360, 480, 600, 720, 1080, 1440 and 2880 min) after the adsorption process commenced. The samples were filtered through a 0.45 μm filter membrane. Subsequently, the concentrations of the residual AgNPs in the solution were assessed to ascertain the adsorbed quantity q_t of AgNPs on SMP at various time intervals. The equation used for the calculation is as follows:

$$q_t = \frac{(C_0 - C_t)V}{m} \quad (1)$$

In this study, q_t (mg g^{-1}) represents the amount of AgNPs adsorbed by SMP at time t (min); C_0 (mg L^{-1}) and C_t (mg L^{-1}) denote the initial and residual concentrations of AgNPs at time t, respectively; V (mL) is the volume of the solution; m (g) is the mass of the adsorbent added.[28]

Quasi-first-order dynamics, quasi-second-order dynamics and intra-particle diffusion models were employed to fit the experimental data. The formulas for the model are as follows:

Quasi-first-order dynamics formula:

$$q_t = q_e(1 - e^{-k_1 t}) \quad (2)$$

Quasi-second-order dynamics formula:

$$q_t = \frac{k_2 q_e^{\,2} t}{(1 + k_2 q_e t)} \quad (3)$$

Intra-particle diffusion equation:

$$q_t = k_{ip} t^{0.5} + C \quad (4)$$

In this study, q_e (mg g^{-1}) and q_t represent the adsorbed amount at adsorption equilibrium and at time t, respectively; k_1 (min^{-1}), k_2 (mg g^{-1} min^{-1}), and k_{ip} (mg g^{-1} $min^{-0.5}$) are the adsorption rate constants for the quasi-first-order kinetics, quasi-second-

order kinetics, and intra-particle diffusion models, respectively; C (mg g^{-1}) denotes the thickness of the boundary layer.

2.3.2. Adsorption isotherm. In the isothermal adsorption experiment, the initial concentration of the adsorbent SMP was set at 8.4 mg L^{-1} (TOC), while the initial concentrations of the AgNPs were adjusted to 1.887, 2.264, 2.642, 3.019, 3.397, 3.774, 4.151, 4.529, and 4.906 mg L^{-1}, respectively. The initial pH was maintained at 8. The experiments were performed at three controlled temperatures (15 °C, 25 °C, and 35 °C) using a thermostatic shaking chamber. Samples were collected after shaking at 120 rpm for 24 h. After filtration through 0.45 μm filter membranes, the residual concentrations of the AgNPs in the solutions were determined. The adsorption capacity q_e was then calculated and fitted using the Langmuir and Freundlich models, which are formulated as follows:

Langmuir isotherm formula:

$$q_e = \frac{q_{max} K_L C_e}{1 + K_L C_e} \quad (5)$$

Freundlich isotherm formula:

$$q_e = K_F C_e^{1/n} \quad (6)$$

In this study, q_e represents the amount of AgNPs adsorbed by SMP at adsorption equilibrium; C_e denotes the concentration of AgNPs at adsorption equilibrium; q_{max} (mg g^{-1}) represents the maximum adsorption capacity of the AgNPs on SMP; K_L (L mg^{-1}) and K_F (mg g^{-1}) are the adsorption equilibrium constants specific to the Langmuir and Freundlich models, respectively. Finally, n is an empirical parameter that describes the intensity of the adsorption process.

2.3.3. Adsorption thermodynamics. The Gibbs free energy (ΔG^0, kJ mol^{-1}), enthalpy change (ΔH^0, kJ mol^{-1}), and entropy change (ΔS^0, J mol^{-1} K^{-1}) for adsorption of the AgNPs on SMP were calculated using formulas (7)–(9).

$$\Delta G^0 = -RT \ln K^0 \quad (7)$$

$$\Delta G^0 = \Delta H^0 T \Delta S^0 \quad (8)$$

$$\ln K^0 = \frac{\Delta S^0}{R} - \frac{\Delta H^0}{RT} \quad (9)$$

In this study, R (8.314 J (mol^{-1} K^{-1})) denotes the ideal gas constant; K^0 refers to the adsorption dispersion coefficient, which is obtained by plotting $\ln(q_e/C_e)$ *versus* q_e. The y-intercept of the fitted linear equation from this plot corresponds T to $\ln K^0$; (°C) denotes the reaction temperature.

2.4. Characterization of mechanism of SMP resistance to AgNPs

The SMP solution after reaction with AgNPs was subjected to freeze-drying, followed by characterization using scanning electron microscopy (SEM),[29] Fourier-transform infrared (FTIR), and X-ray photoelectron spectroscopy (XPS).

2.4.1. SEM analysis. The apparent morphology of the SMP before and after reaction with the AgNPs was observed using SEM (Nova Nano SEM 450, FEI, Netherlands). The accelerating voltage was set to 10 kV. The freeze-dried samples were attached to conductive adhesive on the sample stage and then sputter-coated with gold. SEM images were acquired at magnifications ranging from 500 00× to 1 000 00×.

2.4.2. FTIR. Infrared spectral characterization was performed using a FTIR instrument (Thermo Fisher Scientific, USA) with the KBr pellet method. The samples were freeze-dried for 48 h and ground, mixed with KBr in a ratio of 1 : 100, then pressed into pellets. Spectra were recorded in the range of 500–4000 cm^{-1}.

2.4.3. XPS analysis. XPS (Escalab 250 Xi, Thermo Fisher Scientific, USA) was used to analyse the elemental composition of C, N, and O in SMP before and after interaction with the AgNPs. The pass energy was 20 eV for the narrow scan and 100 eV for the broad survey scan, with step sizes of 0.05 eV and 1 eV, respectively. The obtained spectra were fitted and analysed using Avantage software.

2.5. Experimental design of influencing factors

In the experiment evaluating the effect of pH, the initial concentrations of the SMP and AgNPs were 8.4 mg L^{-1} and 3.774 mg L^{-1}, respectively. The solution pH was adjusted to 2.0, 3.0, 4.0, 5.0, 6.0, 7.0, 8.0, 9.0, and 10.0 using HNO_3 and NaOH. After shaking for 90 min, the samples were analysed using a UV-vis spectrophotometer in the wavelength range of 200–800 nm. The absorbance of the AgNPs in the solution was measured, and the adsorption capacity for the AgNPs on SMP was subsequently calculated.

In the experiment evaluating the effect of Na^+ and Ca^{2+}, the pH was maintained at 6.0 ± 0.1. The initial concentrations of the SMP and AgNPs were 8.4 mg L^{-1} and 3.774 mg L^{-1}, respectively. The concentrations of Na^+ and Ca^{2+} were set at 1, 2, 5, 8, 10, 20, 30, 50, and 100 mM. After shaking for 90 min, the samples were analysed using a UV-vis spectrophotometer in the wavelength range of 200–500 nm. The absorbance of the AgNPs in the solution was measured, and the adsorption capacity for the AgNPs on SMP was subsequently calculated.

A zeta potential (ζ) analyser (ZETA-check, Anton Paar, AT) was used to measure the surface charge of the AgNPs. Prior to measurement, an appropriate volume of AgNPs solution was taken, and the pH was adjusted to 7 using HCl and NaOH. The surface charge was determined using a He–Ne laser (633 nm) as the light source, with the detection angle set at 90°.

3. Results and discussion

3.1. Apparent variations in morphology of SMP

Fig. 1 illustrates the SEM images of SMP before and after adsorption of the AgNPs. Prior to interacting with the AgNPs (Fig. 1(a) and (b)), SMP exhibited a compact, laminar structure with distinct angular features and multiple, irregular surface protrusions. This morphology contributed to the higher specific surface area, thereby providing abundant active sites for adsorption.[24]

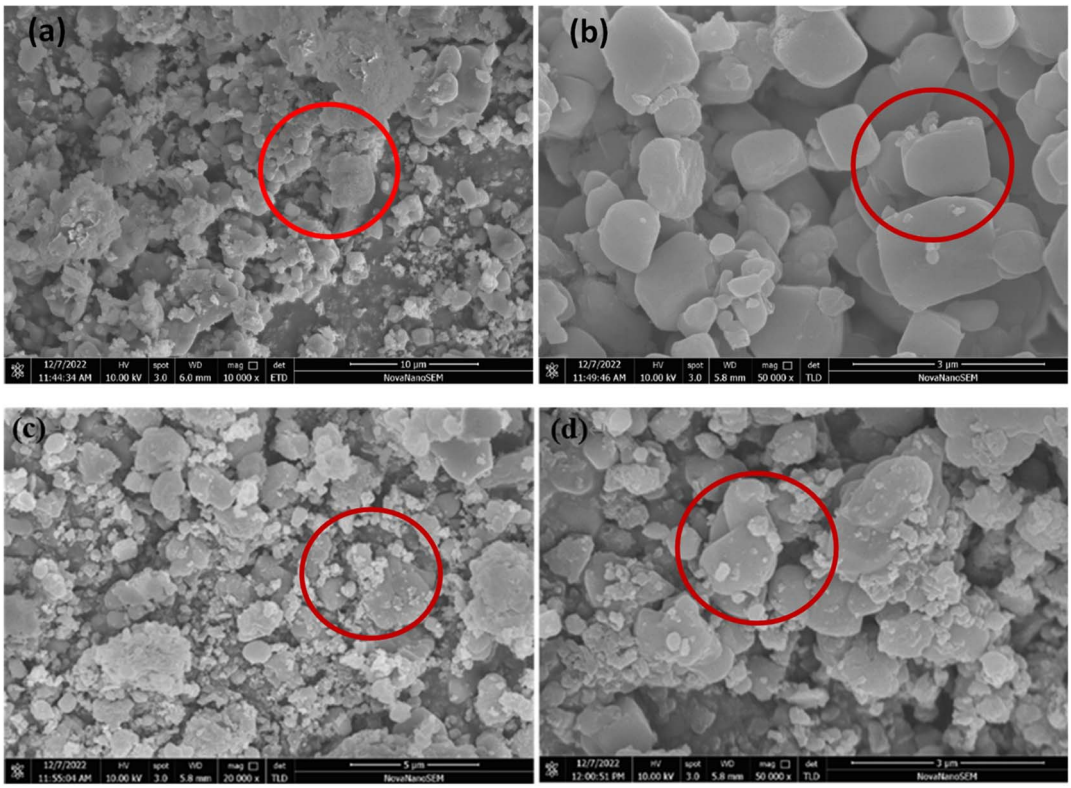

Fig. 1 SEM images of SMP before ((a) 100 00× magnification, (b) 500 00× magnification) and after ((c) 200 00× magnification (d) 500 00× magnification) adsorption of AgNPs.

After interaction with the AgNPs (Fig. 1(c) and (d)), a large number of tiny particles was disorderedly aggregated on the block-like structure of the SMP surface. The boundaries of the SMP became indistinct, surface flocculation was evident, and the overall morphology appeared disrupted. These SEM observations indicate that the unique structural characteristics of SMP not only facilitated effective adsorption of the AgNPs, but also enabled further chelation with them.[30]

3.2. Adsorption mechanism of AgNPs on SMP

3.2.1. Adsorption kinetics. The adsorption variation curves for the AgNPs on SMP at the initial AgNPs concentrations of 3.774 mg L^{-1}, 6.290 mg L^{-1}, and 9.435 mg L^{-1} at 25 °C are shown in Fig. 2(a). During the initial stage of adsorption (0–120 min), SMP components rich in proteins, humic acids, and polysaccharides provided abundant sites for AgNPs, leading to a rapid increase in the adsorbed amounts. Higher initial concentrations of AgNPs induced a steeper concentration gradient between the solution and the adsorbent surface, thereby accelerating the rate of adsorption.[31] As the reaction progressed, the rate of adsorption slowed down and gradually approached equilibrium. The equilibrium adsorption capacities corresponding to the initial concentration were 167.94, 356.17, and 580.05 mg L^{-1}, respectively. Throughout the process, the adsorbed amounts reached 60% of the equilibrium at 200 min and 90% at 960 min, exhibiting a typical "fast adsorption–slow equilibrium" behaviour.[32]

The results of the kinetics experiments were fitted using quasi-first-order and quasi-second-order kinetics models, the fitting curves and relevant parameters are shown in Fig. 2(b) and (c), respectively. The quasi-second-order model had a higher correlation coefficient ($R_2^2 = 0.9948$) than the quasi-first-order model ($R_1^2 = 0.9473$). Moreover, the theoretical equilibrium adsorption capacity q_e predicted by the quasi-second-order model was in better agreement with the experimental value q_{exp}. These results suggest that the adsorption of AgNPs onto SMP in activated sludge predominantly follows quasi-second-order kinetics, indicating that the process is mainly governed by chemisorption, with physical adsorption also contributing.

The fitting results for adsorption of the AgNPs onto SMP using the intraparticle diffusion kinetics model are presented in Fig. 2(d) and the fitting parameters are listed in Table 1. The adsorption process could be divided into three distinct phases based on the model. In the first stage (0–240 min), the adsorption rate was significantly higher than that in the subsequent two stages, as evidenced by the rate constants ($k_{ip1} > k_{ip2}$ and $k_{ip1} > k_{ip3}$). At the end of this initial phase, the adsorption amounts accounted for 66.4%, 91.4%, and 84.1% of the total adsorption, respectively. In the second and third stages, the fitted curves did not pass through the origin, indicating that the rate-limiting step did not involve intraparticle diffusion alone, but also involves other processes such as film diffusion and aggregate precipitation. Additionally, the

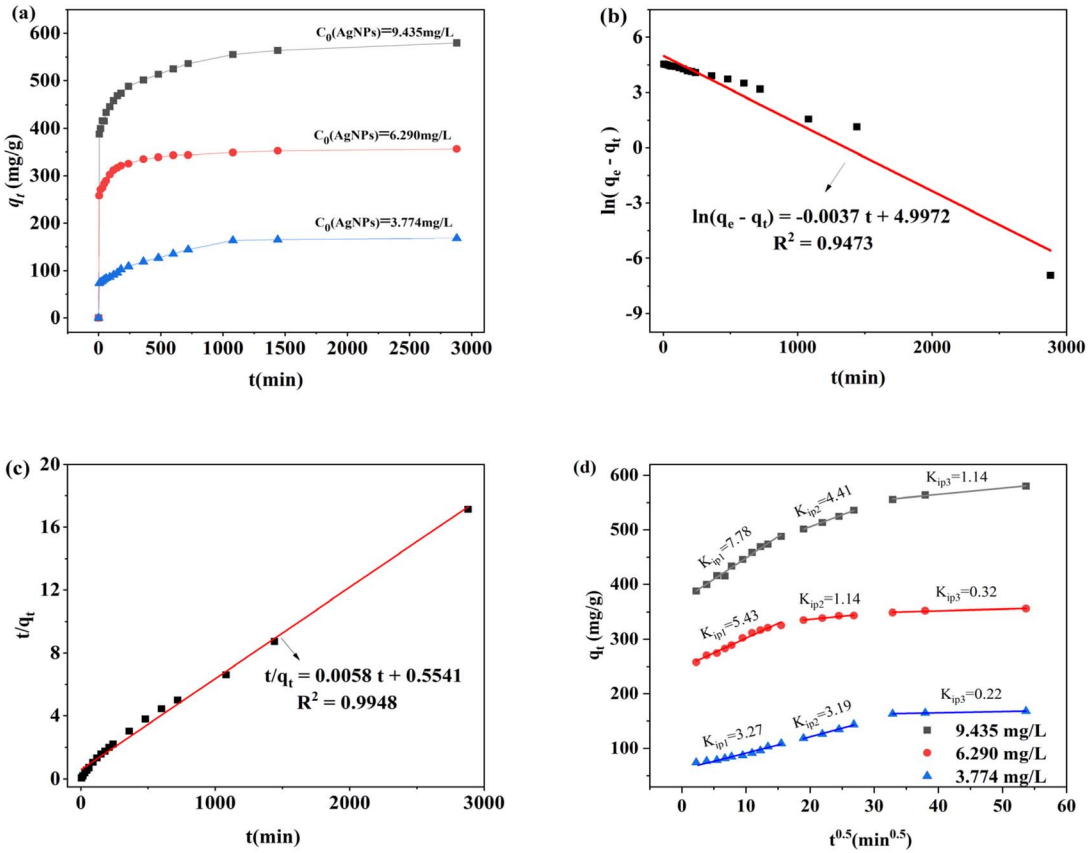

Fig. 2 (a) Variation curves for SMP adsorption amount at different initial AgNPs concentrations; (b) quasi-first-order dynamics and (c) quasi-second-order dynamics fitting results for adsorption of AgNPs on SMP; (d) intra-particle diffusion model fitting results for adsorption of AgNPs on SMP.

Table 1 Kinetic parameters of the in-particle diffusion model for SMP adsorption of AgNPs

C_0 (mg L^{-1})	k_{ip1} (mg g^{-1} $min^{-0.5}$)	C_1 (mg g^{-1})	k_{ip2} (mg g^{-1} $min^{-0.5}$)	C_2 (mg g^{-1})	k_{ip3} (mg g^{-1} $min^{-0.5}$)	C_3 (mg g^{-1})
3.774	3.27	49.53	3.19	57.31	0.22	156.03
6.290	5.43	247.65	1.14	313.88	0.32	339.23
9.435	7.78	370.65	4.41	417.33	1.14	519.21

intraparticle diffusion intercept constant (C_i) was relatively large,[33] further confirming that the surface boundary layer had a substantial impact on the overall adsorption process.[34] Therefore, reducing the thickness of the surface boundary layer could potentially mitigate the impact of film diffusion.[35]

3.2.2. Adsorption thermodynamics

3.2.2.1 Adsorption isotherm. The adsorption behaviour of the AgNPs on SMP was evaluated using the Langmuir and Freundlich adsorption isotherm models. The fitting curves and corresponding parameters are shown in Fig. 3(a) and (b) and are summarized in Table 2. Based on comparison of the R^2 values, the Freundlich model (R^2 = 0.9392, 0.9159, and 0.9308, respectively) fitted the experimental data more accurately, indicating that multilayer adsorption was the predominant mechanism of uptake of the AgNPs by SMP in activated sludge. The Freundlich constant $1/n$ ranged between 0 and 1, suggesting an adsorption process.[36]

3.2.2.2 Adsorption thermodynamics. The changes in the adsorption capacity of the AgNPs on SMP at 15 °C, 25 °C, and 35 °C and the thermodynamic parameters of the adsorption process are shown in Fig. 3(c) and Table 3, respectively. $\Delta H^0 > 0$ indicates that the adsorption of the AgNPs on SMP is an endothermic process. $\Delta G^0 < 0$ and $\Delta S^0 > 0$ suggest that the adsorption process is spontaneous and leads to an increase in the entropy. Moreover, the absolute value of ΔG^0 increased with rising temperature, indicating that elevated temperatures enhanced the spontaneity of the adsorption reaction.

In summary, the adsorption of AgNPs onto SMP in activated sludge was characterized as a spontaneous, endothermic process accompanied by increased system disorder. Elevated temperature facilitated the adsorption reaction. The maximum adsorption capacities of SMP for the AgNPs were 238, 245, and 270 mg g^{-1} at 15, 25, and 35 °C, respectively. Previous studies have reported that Fe_3O_4-loaded activated carbon derived from

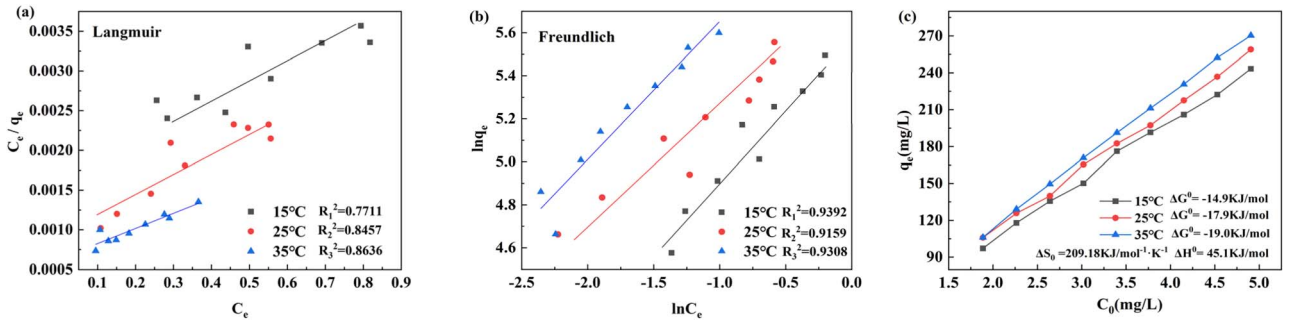

Fig. 3 Isothermal adsorption fitting of AgNPs on SMP at different temperatures: (a) Langmuir and (b) Freundlich. (c) Variations in the adsorption amount of AgNPs on SMP at different initial temperatures.

Table 2 Adsorption isotherm fitting parameters for AgNP adsorption on SMPs at different temperatures

Temperature	Langmuir isotherm			Freundlich isotherm		
T (°C)	K_L (L mg^{-1})	q_m (mg g^{-1})	R^2	K_F	$1/n$	R^2
15	270.4	270.4	0.7711	273.6	0.70	0.9392
25	357.3	357.3	0.8457	309.5	0.49	0.9159
35	525.8	525.8	0.8636	542.2	0.64	0.9308

Table 3 Adsorption thermodynamic parameters for AgNP adsorption on SMPs

T (°C)	ΔG^0 (KJ mol^{-1})	ΔH^0 (KJ mol^{-1})	ΔS^0 (KJ mol^{-1-1} K^{-1})
15	−14.9	45.1	209.18
25	−17.9		
35	−19.0		

pistachio shells exhibited a maximum adsorption capacity of 119.04 mg g^{-1} for Cd^{2+},[37] while magnetically modified halloysite showed a maximum adsorption capacity of 67.9 mg g^{-1} for AgNPs.[38] These comparisons highlight that SMP is an effective adsorbent for AgNPs. As a soluble adsorbent surrounding the microorganisms in activated sludge systems, SMP can mitigate the cytotoxicity of AgNPs through adsorption, acting as the first line of resistance.

3.3. Bonding mechanism of AgNPs on SMP

3.3.1. FTIR characterization. Comparison of the infrared spectra of SMP before and after the reaction with AgNPs revealed a shift in the –OH stretching band of the carboxylic acid (derived from humic acid substances) at 2362 cm^{-1} with concurrent enhancement of the vibrational intensity (Fig. 4(a)). This phenomenon indicates the presence of hydrogen-bonding and electrostatic interactions between SMP and AgNPs.[39] Additionally, the combined spectral peak of –OH and –NH_2 (at 3398 cm^{-1}) shifted by 52 cm^{-1} towards the longer wavelength region. Meanwhile, the intensity of the absorption peaks increased significantly. These observations suggest that the O–H and N–H bonds in SMP formed hydrogen bonds with the Ag^+ ions released from the AgNPs.[40] The stretching vibrational peaks corresponding to C=O and C–N in the amide I band of the protein at 1649 cm^{-1} and 1387 cm^{-1}, respectively, almost completely disappeared. This disappearance might be attributed to the fact that the electron-rich N and O atoms chelated with Ag^+ during the reaction process. As a result, new chemical bonds such as N–O bonds and –OH bonds were formed.[41] Moreover, the absorption peaks in the range of 1060 cm^{-1} to 510 cm^{-1}, together with the absorption peak of the C–O stretching vibration at 1140 cm^{-1}, indicate that functional groups including alcohols, phenols, and polysaccharides in SMP participated in bonding to the AgNPs.[42] Functional groups including –COOH, –OH, and –C=O served as effective binding sites for metal ions.[43,44] These results demonstrate that SMP interacted with the AgNPs through functional groups such as –OH and –NH_2, commonly found in alcohols, phenols, and polysaccharides, *via* hydrogen bonding, electrostatic interactions, and other mechanisms. Hydrogen bonding was confirmed to be the main interaction mechanism between SMP and the AgNPs.[45] Furthermore, O- and N-containing functional groups were capable of removing heavy metal ions through chelation and ion exchange processes.[46] Therefore, protein-derived amides could further chelate with the AgNPs, resulting in the formation of N–O and –OH bonds.[47]

3.3.2. XPS characterization. The changes in the XPS spectra (C spectra, N spectra and O spectra) before and after the reaction of SMP with the AgNPs are shown in Fig. 4.

After the interaction of SMP with the AgNPs (Fig. 4(b) and (c)), the peak areas corresponding to C–C, π–π, and C=O/C–O decreased by 51.8%, 16.5%, and 4.4%, respectively. These changes, in combination with the alteration of the half-peak widths, suggest a significant shift in the chemical environment of the C elements. The data indicate that all three C-containing bonds were involved in the interaction with the AgNPs.[48] During the interaction, O in the functional groups donated electrons to the AgNPs, leading to a decrease in the electron density of the C-containing bonds.[49] Consequently, the binding energies of C=O and C–O increased from 288.8 eV to 288.96 eV.

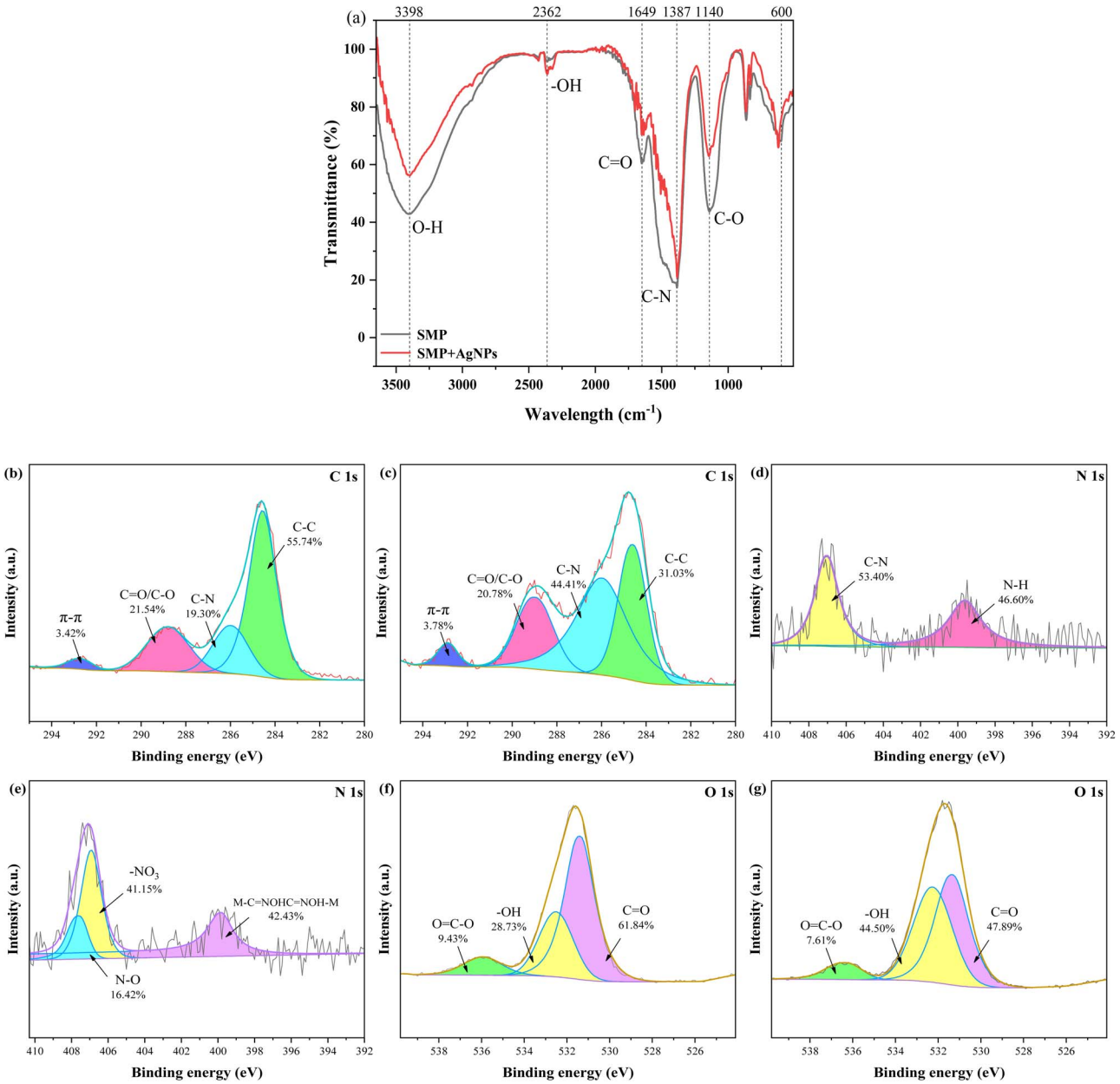

Fig. 4 FTIR spectra of SMP before and after defence against AgNPs (a). XPS spectrum of SMP before and after defence against AgNPs: (b) and (c) C spectrum analysis; (d) and (e) N spectrum analysis; (f) and (g) O spectrum analysis.

The N spectrum of SMP (Fig. 4(d) and (e)) displayed two peaks (C–N and N–H), which disappeared after interaction with the AgNPs, where new peaks appeared: (i) N–O at 407.58 eV; (ii) $-NO_3$ at 406.93 eV; (iii) M-C=NOHC = NOH structure at 339.85 eV. The findings suggest that both C–N and N–H in proteins participated in reactions with Ag^+ released by the AgNPs, donating electrons to Ag^+. This electron donation increased the binding energy, leading to the disappearance of the original C–N and N–H peaks and formation of N–O and $-NO_3$.[50] Moreover, N–O and $-NO_3$ participated in chelation with the metal as the ligands, and the M–C=NOHC=NOH structure was formed, which supported the close association between M–C=NOHC=NOH formation and chelation.[51] Taken together, the peptide bonds and amide compounds in SMP played a pivotal role in counteracting the AgNPs,[52] converting 42.43% of the nitrogen-containing groups into metal chelates and thereby facilitating AgNP removal, consistent with the FTIR analysis.

The O spectrum of SMP (Fig. 4(f) and (g)) displayed three peaks: (i) C=O; (ii) –OH; (iii) O=C–O. After interacting with the AgNPs, the binding energy of C=O remained unchanged, but its peak area decreased from 44 766.2 AU*min to 41 734 AU*min, and the half-peak width increased from 1.67 eV to 1.87 eV, indicating a physical adsorption interaction between C=O and the AgNPs.[53] The peak area of –OH at 532.51 eV increased from 20 798.5 AU*min to 38 784.4 AU*min, likely due

to cleavage of the O=C–O bonds and subsequent formation of additional –OH groups. The peak area of O=C–O decreased at 535.95 eV, with the half-peak width decreasing from 2.2 eV to 1.72 eV, and the binding energy increasing from 535.95 eV to 536.32 eV. Thus, the above analyses indicate chemisorption of AgNPs *via* the O=C–O groups.[53]

Based on the aforementioned analysis, SMP chemically interacted with the AgNPs *via* C–C, C=O/C–O, π–π, O=C–O, C–N, and N–H bonds. C–N and N–H in proteins were entirely engaged in the chemical reactions, and were oxidized to form N–O and $-NO_3$. Meanwhile, the metal-bound form of the oxides, M-C=NOHC=NOH–M, was also produced, inducing conformational changes in the SMP-derived proteins.[54] Physisorption occurred between C=O and the AgNPs. Therefore, the adsorption of the AgNPs onto SMP involved multiple binding mechanisms, including electrostatic attraction, complexation, ion exchange, and surface precipitation.[55]

3.4. Effect of pH and ionic strength on SMP resistance to AgNPs

3.4.1. Effect of pH on SMP resistance to AgNPs. The adsorption amount of the AgNPs on SMP, the absorbance of the AgNPs and the ζ of the solution at different pH values are shown in Fig. 5.

The ζ of the AgNPs was −6.3 mV and −44.2 mV at pH 2 and 3, respectively. Because stabilization of the ζ of AgNPs requires $|\zeta| > 40$ mV,[56] the AgNPs were unstable at pH = 2 to 3, with most existing as precipitates.[57,58] Consequently, the absorbance of the AgNPs in solution was as low as 0.16 and 0.34 at these pH values. Despite this, the adsorption amounts of the AgNPs on SMP reached 52.9 mg g^{-1} and 178.2 mg g^{-1}. Correspondingly, the absorbance decreased by only 0.08 and 0.18 after the adsorption process.

At pH 4–10, the ζ of the AgNPs was in the range of 47.4–47.8 mV, indicating that the AgNPs were in a steady state.[59] As the pH increased, the adsorption capacity of the AgNPs on SMP gradually rose from 234.1 mg g^{-1} at pH 4 to 263.9 mg g^{-1} at pH 10. This trend is attributed to the fact that SMP interacted with the AgNPs primarily through adsorption and complexation, particularly involving phenolic hydroxyl groups, which required the participation of OH^-.[60] While AgNPs were consumed by the action, the ionic equilibrium was shifted towards the direction of increasing concentration, resulting in the absorbance of the AgNPs in solution fluctuating within the range of 0.34–0.35, maintaining a relatively stable state.

Relevant studies have shown that the pH range of urban combined domestic wastewater in China is 6.5–8.5.[55] Within this pH range, the adsorption capacity of the AgNPs on SMP was 249.8–253.2 mg g^{-1}, indicating relatively high adsorption performance. Therefore, SMP can be considered an excellent natural adsorbent for mitigating AgNPs in activated sludge systems, thereby enhancing the *in situ* removal efficiency of AgNPs.

3.4.2. Effect of Na^+ and Ca^{2+} on SMP resistance to AgNPs. In the study of the effects of Na^+ and Ca^{2+}, with increasing concentrations of Na^+ and Ca^{2+}, the UV-vis absorption peaks of the AgNPs gradually weakened and eventually disappeared (Fig. 6). Specifically, when the concentrations of Na^+ and Ca^{2+} reached 50 mM and 1 mM, respectively, the absorption peaks of the AgNPs essentially vanished. These results indicate that the addition of metal cations in the solution facilitated the removal of the AgNPs by SMP,[61] and the higher the cation concentration, the more pronounced the promoting effect. This is due to the increase in the absolute ζ value of the system at high ionic strength, which destabilized the citrate-coated AgNPs and accelerated the adsorption by large-molecule SMP.[62]

Compared to Na^+, Ca^{2+} was more effective in promoting the adsorption of the AgNPs by SMP. This is presumably because Ca^{2+} can react with functional groups such as carboxyl in SMP to form long-chain polymeric organics, which could act as a mediator to promote the aggregation and removal of the AgNPs through adsorption bridging.[63]

3.5. Mechanism by which SMP exhibits resistance against AgNPs

According to the above analysis, the AgNPs were adsorbed onto the surface of SMP through physical interactions such as van der Waals force, forming a multimolecular adsorption layer (Fig. 7). The functional groups in SMP, including –OH, –COOH, and –C=O, provided binding sites for metal ions, enabling the adsorption of the AgNPs on SMP to reach 245 mg g^{-1} at 25 °C. Beyond physical adsorption, these groups (such as C–C, C=O/

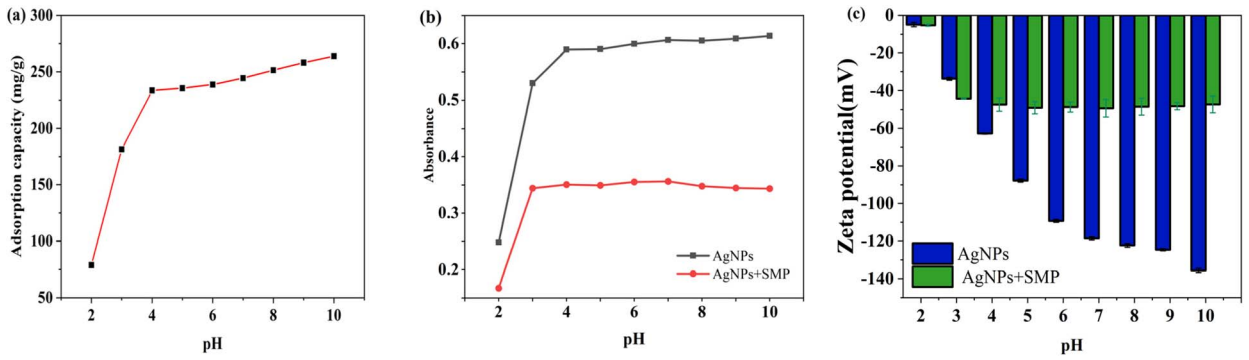

Fig. 5 (a) Adsorption amount of AgNPs on SMP at different pH values; (b) UV absorbance of AgNPs at different pH values; (c) zeta potentials of adsorbed solutions at different pH values.

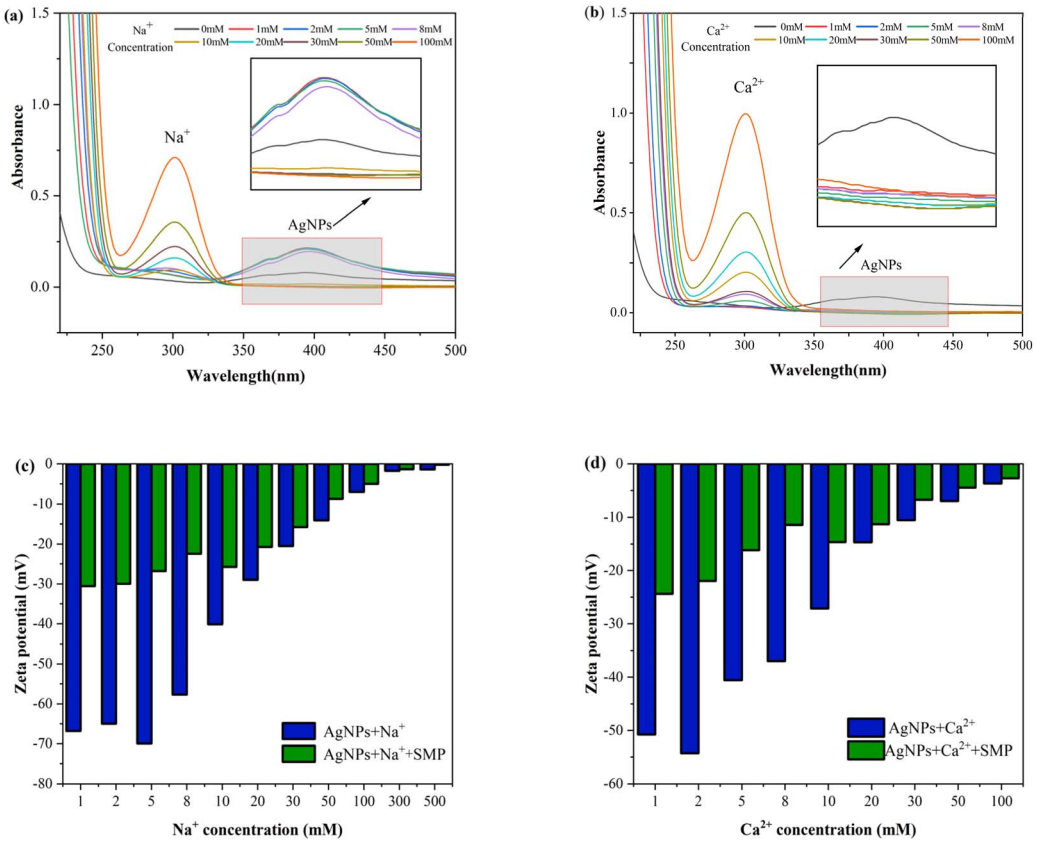

Fig. 6 UV absorbance variations of AgNPs during adsorption from solutions with different Na^+ (a) and Ca^{2+} (b) strengths; zeta potential variations of AgNPs during adsorption from solutions with different Na^+ (c) and Ca^{2+} (d) strengths.

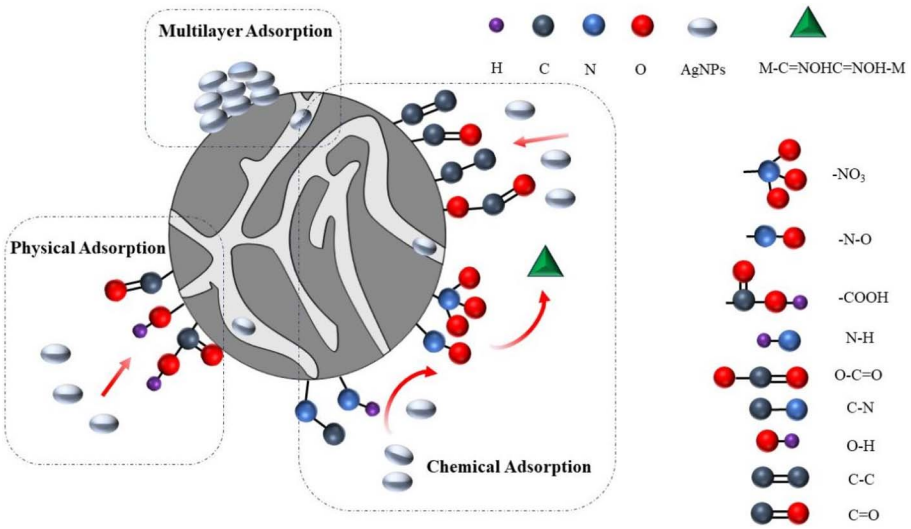

Fig. 7 Schematic representation of the resistance mechanism of SMP against AgNPs.

C–O, O═C–O, C–N, π–π, and N–H) chemically interacted with the AgNPs *via* hydrogen bonding and specific chemical interactions. Among these, N–H and further chelated into oxides in the metal-bound form of M–C═NOHC═NOH–M, resulting in conformational changes in the SMP-derived proteins. In addition, both elevated pH and ionic strength in solution led to a higher adsorption affinity of SMP for the AgNPs. Compared with low-valence metal ions, high-valence metal ions were more effective in promoting the interaction between SMP and the AgNPs.

4. Conclusions

The study investigated the mechanism by which SMP exhibits resistance to AgNPs in activated sludge and yielded the following findings:

(1) The adsorption of AgNPs on SMP conformed to the quasi-second-order reaction kinetic equation. This process was primarily dominated by chemical adsorption and multilayer adsorption, with concurrent physical adsorption. The adsorption is characterized by "fast adsorption–slow equilibrium." The maximum adsorption amount of the AgNPs on SMP was 238 mg g^{-1}, 245 mg g^{-1}, and 270 mg g^{-1} at 15 °C, 25 °C, and 35 °C, respectively. These results demonstrate that SMP is a significant, naturally occurring adsorbent in activated sludge systems, capable of effectively adsorbing and removing AgNPs.

(2) SMP underwent a chemical reaction with the AgNPs through various functional groups (including C–C, π–π, C═O/C–O, O═C–O, C–N, and N–H), where hydrogen bonding mediated the primary mechanism. Following the reaction, the C–N and N–H groups within SMP were oxidized, forming N–O and $–NO_3$ compounds. This was accompanied by chelation processes, resulting in the formation of metal–organic chelates with the structure M–C═NOHC═NOH–M. These transformations ultimately induced conformational changes in the proteins present within SMP.

(3) Increasing the pH and ionic strength of the metal ion enhanced the adsorption of AgNPs by SMP. Compared with Na^+, Ca^{2+} led to more pronounced enhancement of the adsorption capacity of SMP for the AgNPs. Thus, SMP in activated sludge systems can effectively retain AgNPs under typical pH conditions of municipal wastewater in China.

Author contributions

J. K.: Data curation, investigation, methodology, writing – original draft, writing – review & editing. A. W. and Y. Z.: Data curation, investigation, methodology, writing – original draft. F. D. and J. Z.: Data curation, investigation, methodology. C. S.: Data curation, writing – original draft. G. S.: Supervision, writing — review & editing. All authors have agreed to their individual contributions.

Conflicts of interest

The authors declare that they have no known competing financial interests or personal relationships that could have appeared to influence the work reported in this paper.

Data availability

The authors confirm that the data supporting the findings of this study are available within the article.

Acknowledgements

This work was supported by the Henan Provincial Higher Education Key Scientific Research Project Programme (24B560011) and the Key Promotion Project of Henan Province (No. 252102321173). We also thank ZhongZhou Water Holding Co., Ltd for supporting this study.

References

1 X. Huangfu, Y. Xu and R. Huang, *Chemosphere*, 2019, **219**, 766–783.
2 A. Zeng, R. Yang, Y. Tong and W. Zhao, *Int. J. Biol. Macromol.*, 2023, **235**, 123739.
3 C. Forstner, T. G. Orton, P. Wang, P. M. Kopittke and P. G. Dennis, *Environ. Sci. Technol.*, 2020, **54**(21), 13538–13547.
4 N. Li, S. Zhu, C. Wen, H. Xu, C. Li, S. Zhu, R. Li, L. Chen and X. Luo, *J. Water Process Eng.*, 2023, **56**, 104256.
5 A. Syafiuddin, S. Salmiati, T. Hadibarata, A. B. H. Kueh, M. R. Salim and M. A. A. Zaini, *Sci. Rep.*, 2018, **8**(1), 986.
6 J. Huang, C. Yan, J. Liu, W. Guan, R. P. Singh, C. Cao and J. Xiao, *J. Environ. Manage.*, 2019, **245**, 28–36.
7 E. McGillicuddy, I. Murray, S. Kavanagh, L. Morrison, A. Fogarty, M. Cormican, P. Dockery, M. Prendergast, N. Rowan and D. Morris, *Sci. Total Environ.*, 2019, **575**, 231–246.
8 P. H. Zadeh, A. Serrano, G. Collins and F. G. Fermoso, *Ecotoxicol. Enviro. Safe.*, 2022, **238**, 113579.
9 Z. Z. Zhang, Q. Q. Zhang, J. J. Xu, R. Deng, Z. Q. Ji, Y. H. Wu and R. C. Jin, *Bioresource Technol.*, 2016, **200**, 208–216.
10 J. Kang, G. Du, X. Gao, B. Zhao and J. Guo, *Water Environ. Res.*, 2014, **86**(3), 223–231.
11 Z. Guo, L. Ma, Q. Dai, Y. Liu, D. Zhang and R. Ao, *J. Environ. Manage.*, 2023, **342**, 118287.
12 P. Wang, D. Sun, M. Deng, S. Zhang, Q. Bi, W. Zhao and F. Huang, *Environ. Sci.-Nano*, 2020, **7**(4), 1266–1274.
13 M. W. Yasir, M. B. A. Siddique, Z. Shabbir, H. Ullah, L. Riaz and A. A. Shah, *Sci. Total Environ.*, 2019, **779**, 146345.
14 Z.-Z. Zhang, R. Deng, Y.-F. Cheng, Y.-H. Zhou, X. Buayi, X. Zhang, H.-Z. Wang and R.-C. Jin, *J. Hazard. Mater.*, 2015, **300**, 838–846.
15 F. Çeçen, A. G. Geyik and B. Kılıç, *Water, Air, Soil Pollut.*, 2020, **231**, 1–13.
16 G. F. Li, W. J. Ma, Y. F. Cheng, S. T. Li, J. W. Zhao, J. P. Li, Q. Liu, N. S. Fan, B. C. Huang and R. C. Jin, *Chem. Eng. J.*, 2020, **393**, 124800.
17 S. Lu, X. Li, Y. Xi, H. Liu, Z. Zhang, Y. Huang, T. Xie, Y. Liu, B. Quan and C. Zhang, *J. Colloid Interf. Sci.*, 2021, **596**, 408–419.
18 X. F. Sun, S. G. Wang, X. M. Zhang, J. P. Chen, X. M. Li, B. Y. Gao and Y. Ma, *J. Colloid Interf. Sci.*, 2009, **335**(1), 11–17.
19 R. Xu, F. Fang, L. Wang, J. Luo and J. Cao, *J. Environ. Sci.*, 2023, **124**, 130–138.
20 L. Holakoo, G. Nakhla, E. K. Yanfu and A. S. Bassi, *Water Res.*, 2006, **40**(8), 1531–1538.
21 H. Ren, F. Ma, X. Yao, K. Shao and L. Yang, *J. Hydrol.*, 2020, **591**, 125289.
22 Y. Li and X. Gong, *Rev. Environ. Contam. T.*, 2021, **257**, 69–92.
23 P. Hasani Zadeh, F. G. Fermoso, G. Collins, A. Serrano, S. Mills and F. Abram, *Safe*, 2023, **252**, 114604.

24 G. Bayramoğlu and M. Y. Arıca, *Bioresource Technol.*, 2009, **100**(1), 186–193.
25 S. A. Bhat, G. Cui, W. Li, *et al.*, *Chemosphere*, 2020, **241**, 125035.
26 K. Matyja, A. Wasiela, W. Dobicki, *et al.*, *Bioresour. Technol.*, 2021, **339**, 125623.
27 X. Zheng, T. Liu, M. Guo, *et al.*, *Water Res.*, 2020, **179**, 115895.
28 Y. Mata, M. Blázquez, A. Ballester, F. González and J. Muñoz, *J. Hazard. Mater.*, 2010, **178**(1–3), 243–248.
29 S. Şengör and P. Gikas, *J. Global Nest*, 2014, **16**, 699–706.
30 H. Xu, J. Pan, H. Zhang and L. Yang, *Ecol. Eng.*, 2016, **94**, 464–470.
31 M. Verma, W. Ahmad, J. H. Park, V. Kumar, M. S. Vlaskin, D. Vaya and H. Kim, *J. Water Process Eng.*, 2022, **49**, 102989.
32 R. Soto-Ramírez, L. Tavernini, M. G. Lobos, P. Poirrier and R. Chamy, *Algal Res.*, 2023, **74**, 103179.
33 Q. Hu, S. Ma, Z. He, H. Liu and X. Pei, *J. Water Process Eng.*, 2024, **60**, 105241.
34 L. C. Auton, M. Aguareles, A. Valverde and T. G. Myers, *App. Math. Model.*, 2024, **130**, 827–851.
35 S. P. Dharmarathna and N. Priyantha, *Energy Nexus*, 2024, **14**, 100294.
36 J. Yang, W. Wei, S. Pi, F. Ma, A. Li, D. Wu and J. Xing, *Bioresource Technol.*, 2015, **196**, 533–539.
37 V. Islami and M. R. Islami, *Mat. Sci. Eng. C-Mater*, 2019, **101**, 42–52.
38 D. Janacek, L. Kvitek, M. Karlikova, K. Pospiskova and I. Safarik, *Appl. Clay Sci.*, 2018, **162**, 10–14.
39 S. M. N. Gallón, E. Alpaslan, M. Wang, P. Larese-Casanova, M. E. Londoño, L. Atehortúa, J. J. Pavón and T. J. Webster, *Mat. Sci. Eng. C-Mater*, 2019, **99**, 685–695.
40 P. Yan, J. S. Xia, Y. P. Chen, Z. P. Liu, J. S. Guo, Y. Shen, C. C. Zhang and J. Wang, *Bioresource Technol.*, 2017, **232**, 354–363.
41 H. Liu, W. Y. Xie, F. Song, X. L. Wang and Y. Z. Wang, *Chem. Eng. J.*, 2019, **369**, 1040–1048.
42 Y. Li, K. Wang, S. Dötterl, *et al.*, *J. Hazard. Mater.*, 2024, **476**, 135123.
43 M. Moovendhan and R. Srinivasan, *J. Environ. Manage.*, 2023, **335**, 117484.
44 C. J. Tang, M. Abraham, F. Feng, Z.-G. Liu, Y. X. Song, Y.-Y. Wang and X. Tang, *J. Water Process Eng.*, 2021, **41**, 102094.
45 L. Yuan, Y. Wu, Q. Fan, *et al.*, *Sci. Total Environ.*, 2023, **862**, 160872.
46 Y. Na, J. Lee, S. H. Lee, P. Kumar, J. H. Kim and R. Patel, *Polym.-plast. Tech. Mat.*, 2020, **59**(16), 1770–1790.
47 H. A. Alhazmi, M. S. Alam, M. Albratty, *et al.*, *J. Chem.*, 2023, **2023**(1), 2581653.
48 D. Q. Cao, X. Wang, Q. H. Wang, X. M. Fang, J. Y. Jin, X. D. Hao, E. Iritani and N. Katagiri, *J. Membrane Sci.*, 2020, **606**, 118103.
49 V. C. Dinh, C. H. Hou and T. N. Dao, *Chemosphere*, 2022, **293**, 133622.
50 N. Kasera, P. Kolar and S. G. Hall, *Biochar*, 2022, **4**(1), 17.
51 A. Sierraalta, R. Añez and M. Brussin, *Phys. Chem. A*, 2002, **106**(29), 6851–6856.
52 X. Qi, H. Yin, M. Zhu, *et al.*, *Chemosphere*, 2022, **294**, 133733.
53 X. Qiao, L. Hao, H. Ren, *et al.*, *Angew. Chem., Int. Ed.*, 2025, **62**, e202508162.
54 H. Liu, J. Chen, Y. Wang, *et al.*, *Environ. Sci. Technol.*, 2022, **56**(7), 4467–4476.
55 L. Wei, J. Li, M. Xue, S. Wang, Q. Li, K. Qin, J. Jiang, J. Ding and Q. Zhao, *Bioresource Technol.*, 2019, **291**, 121868.
56 R. Dobrowolski, A. Krzyszczak, J. Dobrzyńska, B. Podkościelna, E. Zięba, M. Czemierska, A. Jarosz-Wilkołazka and E. A. Stefaniak, *Biochem. Eng. J.*, 2019, **143**, 202–211.
57 R. Bozbay, Ş. Teke, K. K. Ersoy and N. Orakdogen, *Colloid. Surface. A.*, 2024, **693**, 134060.
58 C. Tang, T. Hu, C. Du, Z. Liao, W. Cheng, F. Wang, X. Hu and K. Song, *Polymers*, 2023, **15**, 2918.
59 I. Fernando and Y. Zhou, *Chemosphere*, 2019, **216**, 297–305.
60 B. Dong, G. Liu, J. Zhou, J. Wang and R. Jin, *J. Hazard. Mater.*, 2020, **383**, 121–190.
61 J. Liu, K. Murphy, M. Winchester and V. Hackley, *Bioanal Chem.*, 2017, **409**, 6027–6039.
62 F. Piccapietra, L. Sigg and R. Behra, *Environ. Sci. Technol.*, 2012, **46**(2), 818–825.
63 L. Zha, J. Hu, C. Wang, S. Fu and M. Luo, *Colloid Polym. Sci.*, 2002, **280**, 1116–1121.